Physics of Plasmas ARTICLE scitation.org/journal/php

Wake excitation by a powerful microwave pulse and its evolution in a plasma-filled waveguide

Cite as: Phys. Plasmas **27**, 053103 (2020); doi: 10.1063/5.0005849
Submitted: 25 February 2020 · Accepted: 18 April 2020 ·
Published Online: 5 May 2020

Y. Cao,[1,a)] Y. P. Bliokh,[1] J. G. Leopold,[1] A. Li,[2] G. Leibovitch,[1] and Ya. E. Krasik[1]

AFFILIATIONS

[1]Physics Department, Technion, Haifa 3200003, Israel
[2]National University of Defense Technology, Changsha 410073, China

[a)]Author to whom correspondence should be addressed: neo.cao.yang@gmail.com

ABSTRACT

We present the results of an experimental, theoretical, and numerical study of short and long time wake, produced by a 0.6 ns, 0.5 GW, 9.6 GHz high power microwave (HPM) pulse propagating in a plasma-filled cylindrical waveguide. The perturbation of the plasma density caused by the ponderomotive force prevents not only the pulse from spreading due to dispersion, but also leads to pulse compression. The high power pulse leaves far behind it a long lived positively-charged plasma whose electrons oscillate in the Coulomb potential well and ionize the background neutral gas over several tens to hundreds of nanoseconds. This leads to long time light emission observed in the experiment. The density of this newly created plasma can exceed many-folds its initial value. The theoretical model shows that as a result of the wake excitation by the propagating HPM pulse, fast electrons are ejected and collected on the waveguide wall. These high energy electrons, pulse compression, and long time light emission are evidence of the wake formation. The results of the experiment, the analytical model, and the numerical simulations are in good agreement.

I. INTRODUCTION

Gigawatt to multi gigawatt power-scale super-radiant backward wave oscillator (SR-BWO) type high power microwave (HPM) sources producing sub-nanosecond timescale pulses have become available in recent years.[1] Such sources, relatively simple and affordable to build, have attracted our attention for use in studying the interaction of HPM pulses with gases and plasmas because they operate in a relatively uncharted regime. We have already been able to demonstrate that when a HPM pulse is focused to a cm scale region in a neutral gas, it produces electron assisted impact ionization followed by the formation of an under-dense plasma channel with over-critical density plasma walls. The latter allows the HPM pulse propagation almost unperturbed in this plasma channel produced by itself.[2]

A short high power electromagnetic pulse propagating through plasma leaves behind it a density perturbation in the form of Langmuir oscillations. The amplitude of these oscillations can be very high and the electric field strength can reach its maximum limit for the case of completely separated charges. This wake-field, excited in a dense plasma by a short powerful laser pulse, is at the heart of new promising methods of charged particles' acceleration.[3,4]

The propagation of a sub-nanosecond long, gigawatt power scale, HPM pulse in underdense plasma[5] is to be considered a physically scaled down situation of laser experiments. Compared to the laser experiments, a HPM pulse propagating in plasma leaves a similar trail but is characterized by much larger temporal and spatial scales and wake fields smaller by several orders of magnitude, too low to be considered in accelerators. On the other hand, this allows the application of much more conventional time- and space-resolved experimental diagnostics to study the dynamics of the perturbed plasma while the wake develops and to compare with simulations.

In order to increase the electromagnetic power density of the available HPM source, we decided to inject a HPM pulse directly into a waveguide. The SR-BWO produces a TM_{01} electromagnetic mode in its cylindrical cavity with a spatiotemporal distribution of the electric fields so that the electric field is either maximal in the radial direction near the conducting cavity walls or in the longitudinal direction on the axis. In this paper, the HPM pulse is injected into a waveguide of the same diameter as the SR-BWO cavity which contains the plasma and the TM_{01} mode is preserved.[6–8] In our analysis, we consider this mode's specific effect on the ponderomotive and Lorentz forces which determine the electron dynamics and the wake formation. In this paper, we present results of a theoretical, numerical, and experimental study of the wake, that is, the longtime plasma dynamics resulting from the HPM pulse traversing it.

II. EXPERIMENTAL SETUP

The SR-BWO which we used in our earlier research,[9] generates a 500 ± 50 MW, ∼0.7 ns [full width half maximum (FWHM)], 9.6 GHz (central frequency) microwave pulse (TM_{01} mode). Let us note here that for this pulse duration, the plasma resonant density is $n_e \approx 2.6 \times 10^{10}\,cm^{-3}$ and the corresponding resonant plasma wavelength is $\lambda = 14$cm. The output of the SR-BWO is connected to a directional coupler[10] [#1 in Fig. 1(a)]. 24 thin (1.5 mm diameter) stainless steel wires spaced azimuthally ∼1 mm apart (geometrical transparency of ∼60%) makeup a cylindrical waveguide of 28 mm diameter, installed coaxially inside a flashboard plasma source and connected to a second coupler [#2, Fig. 1(a)] at its downstream end. Couplers #1 and #2 measure the HPM pulse waveforms entering and leaving the waveguide during a single shot. The plasma source, described in our earlier research,[8] produces a uniform plasma along the entire volume of the waveguide, consisting of four flashboards placed on the inner surface of a 700 mm long and 90 mm diameter stainless steel tube. By changing the time delay between the beginning of the flashboard discharge and the microwave pulse generation, the density of the plasma is varied in the range $10^{10}\,cm^{-3}$–$10^{12}\,cm^{-3}$ when the pulse propagates through the plasma-filled waveguide. The plasma density and its spatial distribution were measured using different electrical, spectroscopic, and microwave methods.[8] The 24 wire waveguide is sufficiently transparent to allow plasma to fill it before the arrival of the HPM pulse, but is practically opaque to microwaves.

Plastic optical fibers [of 2 mm diameter (Edmund optics), covered at their front end by thin aluminum foils and their back ends attached to fast (≤0.5 ns rise time) photo-multiplier-tubes (PMT) (Hamamatsu H10721–01)], were applied to estimate the maximal energy of electrons using NIST data[11] by varying the Al foil thickness and measuring the resulting luminescence induced in the fiber. As shown in Fig. 1(a), these measurements were carried out at the downstream end of the tube, viewing the waveguide upstream, and at two points along the waveguide inside the flashboard tube, side viewing the effect of the propagating HPM pulse. These optical side-fibers were placed inside a 1-mm-thick Cu tube to protect the fiber from other possible sources of light and radiation. The side-fibers, when placed outside the vacuum chamber behind the Perspex window, were also used to study the time evolution of the plasma light emission's intensity. The current and the energy of electrons leaving the waveguide downstream, were measured on a 3 cm diameter graphite collector [see Fig. 1(b)] of a Faraday cup (FC) covered with Al foils [see Fig. 1(b)] of varying thickness.

A fast framing intensified 4QuikE camera (Stanford computer optics) was used to observe the plasma light emission pattern when the HPM pulse propagates through the waveguide. The camera was placed at the output of the tube [see Fig. 1(c)] and is focused at the mid-plane of the waveguide. To protect the camera from the HPM pulse, a water filled filter was placed in front of it.

Two turbo-molecular pumps maintained a background pressure of $\sim 5 \times 10^{-3}$ Pa inside the chamber. Below, we shall refer to this pressure as "vacuum." Using a calibrated Penning vacuum probe installed in a flashboard tube, it was shown that the pressure in this tube increases up 4 Pa within ∼20 μs from the beginning of the discharge of the flashboard. This increase in the pressure is due to intense gas desorption and surface erosion of the flashboard plasma source.

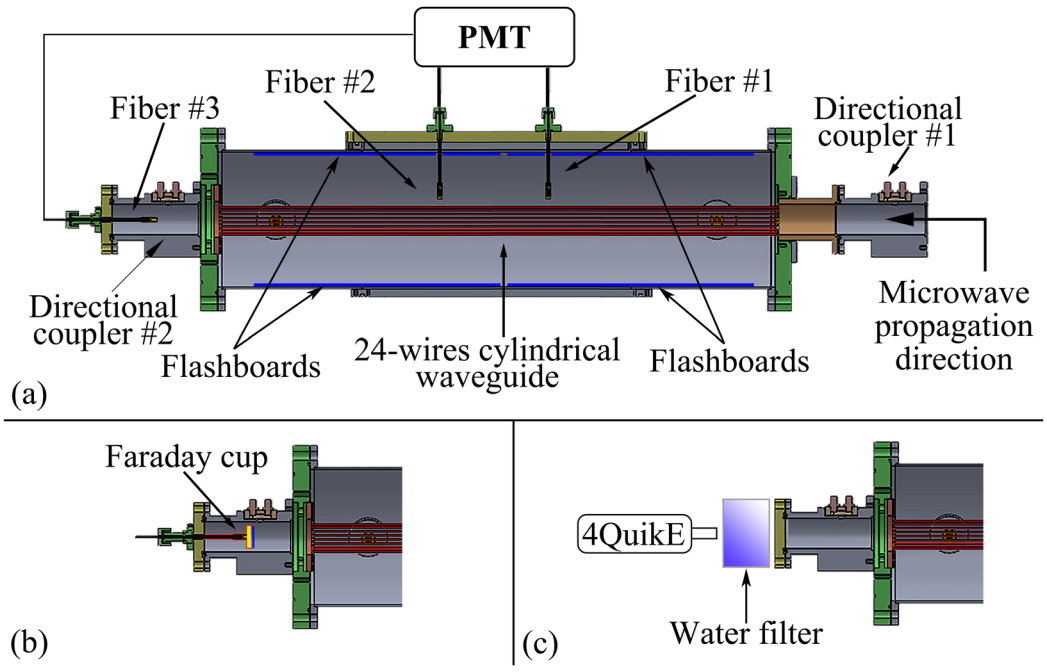

FIG. 1. Schematic drawing of the experimental apparatus. (a) Vacuum chamber containing the 24 wire waveguide. Flashboards along the chamber walls and diagnostic apparatus are pointed out. Enlarged left side end of (a), with either a Faraday cup (b) or with a fast intensified frame 4QuikE camera protected against microwave radiation by a water filter (c) attached to the waveguide end.

III. EXPERIMENTAL RESULTS

Typical plasma-emitted luminosity distributions measured during the propagation of the HPM pulse are shown in Fig. 2. These distributions were obtained by integrating over the pixel intensity distribution of the image obtained by the 4QuickE camera operating with a 1.2 ns frame duration. One can see that the HPM interaction with the plasma changes the observed light emission from almost uniform in the absence of HPM [Fig. 2 (red curve)], to being strongly concentrated near the waveguide axis [Fig. 2 (blue curve)]. Note that no light emission increase is observed by the 4QuickE camera in the absence of plasma, which indicates that ionization of the background gas by the HPM pulse if at all, is negligibly small.

This redistribution of the plasma luminosity cannot be associated with electron–ion collisions because at the plasma densities considered, the electron collision frequency is lower than $10^6\ s^{-1}$. A detailed analysis of the mechanism responsible for the observation seen in Fig. 2 is given in Sec.IV C below.

Typical waveforms obtained by a 20 μm thick Al foil covered FC [Fig. 3(b)] and an 80 μm thick Al foil covered fiber #3 [Fig. 3(c)] in the vacuum and $5 \times 10^{10}\ cm^{-3}$ density plasma for an HPM pulse registered at the entrance to the waveguide by coupler #1 [Fig. 3(a)]. The time difference of ~6 ns between the beginning of the microwave pulse and the electron beam, represents the HPM pulse propagation time through the waveguide and the small time difference between the vacuum and plasma signals represents the effect of the plasma on the propagation time. One can see that high-energy electrons are present in both measurements. In the absence of the plasma, the amplitude and the total duration of the FC signal were smaller than those with the plasma. The origin of the energetic electrons observed in the absence of plasma can be related to the ionization of the residual gas by the propagating HPM pulse. With and without plasma pre-filling, high-energy electrons were detected by the FC covered by Al foils up to 120 μm thickness, that corresponds to electron energies up to 100 keV.[11] The duration and amplitude of the high-energy electron signal decrease with increasing Al foil thickness. The FC signal for electron energies >10 keV was ~1.5 ns long and carried ~80 mA for a plasma density of $n_e \sim 5 \times 10^{10}\ cm^{-3}$.

Induced light emission was also detected in an optical fiber covered by an Al foil when the fiber replaces the FC [Fig. 1(a)]. The light emission waveform registered by the PMT coupled to an 80 μm thick Al foil covered fiber is typically ~3 ns long [Fig. 3(c)]. Luminescence is obtained for up to 140 μm Al foil thickness but with smaller amplitude and shorter duration. These data indicate the presence of downstream electrons of energy ≥100 keV. When a pair of SmCo permanent magnets were placed in front of the fiber, no light was detected. Since the magnets deflect the electrons, this indicates that no other light source is responsible for the registered signal. Here, let us note that the pulses following the main HPM pulse in Fig. 3(a), are the result of imperfect matching between the slow wave structure and the waveguide and that this waveform is reproducible.

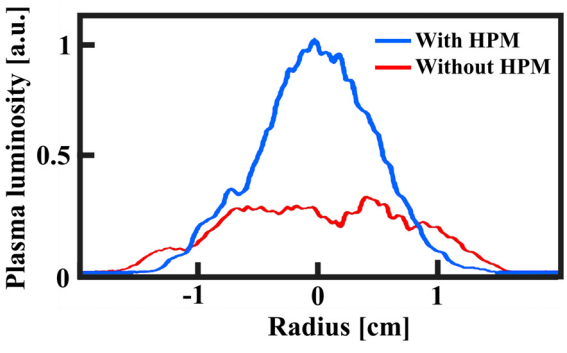

FIG. 2. Plasma luminosity distribution in a $n_e \sim 5 \times 10^{10}\ cm^{-3}$ density plasma (red curve) in the absence of HPM and (blue curve) when the HPM pulse propagates through the plasma. The light distribution in the presence of HPM was obtained at a time delay of ~2.4 ns relative to the moment the pulse enters the waveguide.

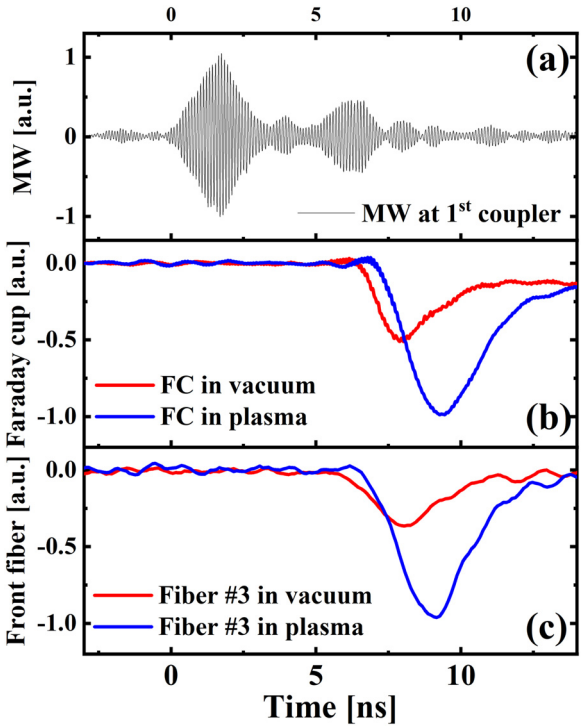

FIG. 3. (a) Normalized MW electric field amplitude waveform measured by coupler #1. (b) Typical waveforms of energetic electron current detected by the FC located at the exit of the waveguide and covered with a 20 μm thick Al foil, in a vacuum (red) and in a $n_e \sim 5 \times 10^{10}\ cm^{-3}$ density plasma (blue) and in (c) the current detected by a 80 μm thick Al foil covered fiber (#3) replacing the FC, in a vacuum (red) and in a $n_e \sim 5 \times 10^{10}\ cm^{-3}$ density plasma (blue).

In experiments with plasma density $n_e > 5 \times 10^{10}\ cm^{-3}$, the maximum amplitude of the electron signal decreases, finally disappearing when the plasma density reaches its cut-off value. As the plasma density decreases below $5 \times 10^{10}\ cm^{-3}$, the signal amplitude also decreases toward that obtained for the vacuum case. We found that the density $5 \times 10^{10}\ cm^{-3}$ is optimal with respect to the results observed in Fig. 3 and other experimental observations, which are discussed below. The origin of the energetic electrons observed in the absence of plasma can be related to the ionization of the residual gas by the propagating HPM pulse.

A typical light emission waveform induced by electrons escaping from the waveguide in the radial direction and penetrating a 20 μm-thick Al foil (corresponding to electron energies of ≥ 10 keV) covered

optical fiber placed radially at a distance of 1.5 cm from the outer diameter of the waveguide and ∼15 cm from the waveguide entry point [Fiber #1 in Fig. 1(a)] and the HPM pulse measured by coupler #1 for a plasma density of 5×10^{10} cm^{-3} are shown in Fig. 4. In Fig. 4, the time-of-flight of the HPM pulse propagation between the coupler #1 to the axial location of the fiber was accounted for. One can see that the high-energy electrons appear at the tail of the HPM pulse. No signal was detected for Al foils exceeding 40 μm thickness, which allows us to estimate the maximum electron energy of the electrons emitted over ∼2 ns to be ∼25 keV. High-energy electrons were not observed in the vacuum, which indicates that HPM induced background electron impact ionization of the background neutral gas is negligible.

The side fibers, placed at the axial distance of 30 cm from each other, when not covered with Al foils were also used to measure the light emitted by the plasma. The time delay between the appearance of light in the two fibers was ∼1 ns, corresponding to the time-of-flight of the HPM pulse along this distance. Typical waveforms of this light intensity obtained by one of these fibers for different plasma densities, are shown in Fig. 5. The light intensity continues to grow during several tens of nanoseconds after the HPM pulse and decays slowly within hundreds of nanoseconds. As mentioned above, ionization of the background gas by the HPM pulse is negligibly small. Therefore, this long time light emission is evidence for the strong perturbation of the plasma left by the HPM pulse in its wake. When the HPM pulse propagated in the vacuum, the same fiber detected a ∼20 times smaller, ≤3 ns long emitted light signal, probably the result of some ionization of the background gas by the propagating HPM pulse.

The waveforms of the incoming and exiting HPM pulse measured by couplers #1 and #2 were compared for different conditions. In the vacuum, the pulse width increases from ∼0.85 ns to ∼1.3 ns, the result of the pulse's dispersion in the waveguide (confirmed by simulations). When the waveguide was filled with ∼10^{11} cm^{-3} density plasma, at coupler #2, the HPM waveform's width compresses and its peak power increases (see Fig. 6). The mechanism responsible for this observation is related to the plasma density modulation produced by the HPM pulse and will be discussed in Sec. IV.

The experimental results presented in this section can be summarized as follows: The interaction of the HPM pulse with plasma (i) redistributes the emitted light from radially-homogeneous to strongly concentrated near the waveguide axis; (ii) it produces strong side light increasing during tens of ns following the pulse and decaying within hundreds of nanoseconds; (iii) radially and axially ejected high-energy electrons are detected; and (iv) the HPM pulse compresses during its propagation through the plasma. These experimental results will be explained theoretically and confirmed numerically in Sec. IV.

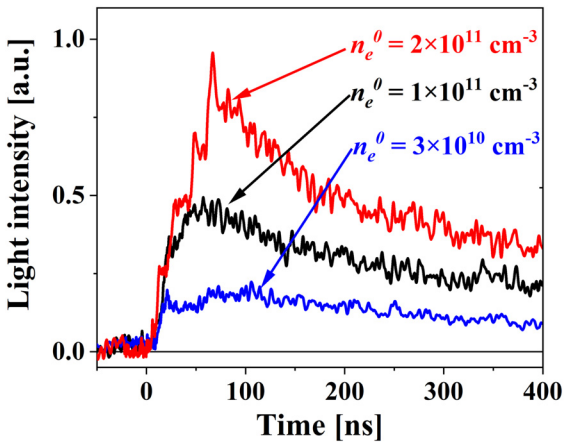

FIG. 5. Light intensity registered by the side fiber for different densities of the plasma fill. Here, time zero corresponds to the arrival time of the HPM to the fiber's axial position.

IV. THEORETICAL ANALYSIS AND NUMERICAL SIMULATIONS

In this section, we use theoretical modeling and numerical simulations to explain the experimental data presented in Sec. III. A simplified one dimensional (1D) model resulting in the plasma density modulation corresponding to a wake excitation in a plasma filled waveguide has been described in Ref. 6. This model does not take into account the axial component of the axial space-charge induced electric field and axial electron motion. More adequate and precise calculations have been performed using a three-dimensional (3D)

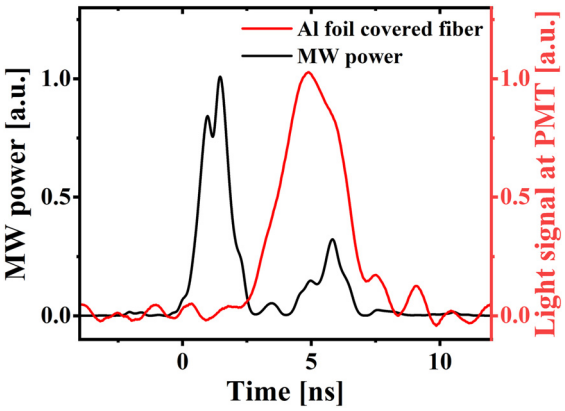

FIG. 4. Typical waveform of the PMT attached to optical fiber #1 covered by a 20 μm-thick Al foil (red) and the HPM power envelope (black) for a plasma density of $n_e \sim 5 \times 10^{10}$ cm^{-3}; $t = 0$ is the arrival time of the HPM pulse to the fiber.

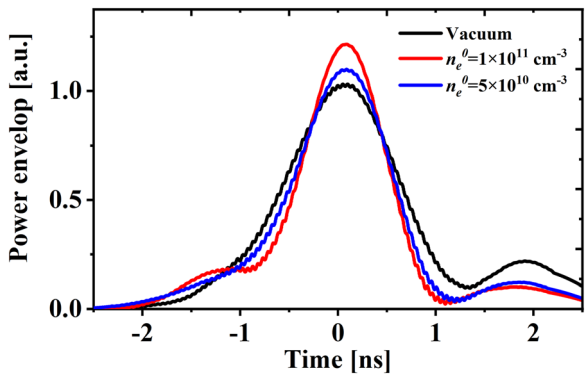

FIG. 6. The HPM power pulse normalized for the vacuum measured by coupler #2 for (black) vacuum, (red) plasma density of 10^{11} cm^{-3}, and (blue) plasma density of 5×10^{10} cm^{-3}. All values are related to the normalized maximum of the power signal measured in the vacuum.

Large-Scale Plasma (LSP) PIC-MCC (particle in cell–Monte Carlo collision) hybrid code.[12,13] There is good qualitative and rather good quantitative agreement between the model and the simulations. All simulations considered only solid wall waveguides so that leaks through the gaps between the wires of the experimental waveguide were neglected.

A. Pulse frequency self-modulation

The ponderomotive force of an HPM pulse ejects electrons from the volume occupied by the pulse, while heavy ions remain immobile. After the pulse has left, the electron oscillations near the equilibrium position continue as a nonlinear Langmuir wave. The displacement of plasma electrons occurs during the presence of the pulse, so that the HPM pulse propagates in a time-dependent medium resulting in the variation of the pulse carrier's frequency. The effect of the frequency shift of a wave propagating through media characterized by non-stationary parameters is well-known and was studied both theoretically[14,15] and experimentally.[16–18]

In early studies, the temporal variation of the plasma density was associated with neutral gas ionization by the propagating HPM pulse[15] or laser beam.[13,16,17] Namely, an increase in the plasma density leads to a frequency up-shift only.[19] In the present experiments, additional ionization can be neglected because the pulse is too short and the preliminary density of the plasma is low. Thus, variations of the pulse spectrum may be associated with the plasma density redistribution caused by the HPM pulse itself. The plasma density perturbation follows the pulse along the waveguide. This situation can be considered as a propagating localized perturbation of the waveguide characteristics. Interaction of the pulse with this co-propagating perturbation can be considered as a particular case of "front-induced transition."[20]

The wake excited by the HPM pulse contains consecutively placed regions of decreasing and increasing electron density regions. Depending on the position inside this wake, the local spectrum of the pulse is red- or blue-shifted. This specific property of the plasma, namely, its effect on the HPM pulse can be used in wakefield "one-shot" diagnostics[21,22] and electromagnetic pulse compression by group velocity dispersion.[23] It is important to note that filamentation and self-focusing, which are typical for the interaction of an electromagnetic pulse with transversally-unbound plasma[24,25] are absent when the plasma is enclosed in a waveguide of radius comparable or less than the wavelength of the electromagnetic wave.

In order to determine the pulse's spectrum variation, let us consider the wake excited by a short TM-mode pulse propagating along a cylindrical waveguide filled with homogeneous plasma. The spatial and temporal variations of the electron density in the wake and the pulse envelope are shown in Fig. 7.

The dispersion equation of the TM mode of a cylindrical waveguide of radius R, filled with homogeneous plasma of density n_0, is given by

$$\omega^2 = c^2k^2 + c^2k_\perp^2 + \omega_p^2 \equiv c^2k^2 + \omega_0^2. \tag{1}$$

Here, k is the longitudinal wave number, $k_\perp = j_{0,i}/R$, $j_{0,i}$ is the i-th root of Besssel function J_0, and ω_p is the plasma frequency $\omega_p^2 = 4\pi e^2 n_0/m$. Note that ω_0 is an eigen-frequency of the two-dimensional resonator formed by the waveguide cross section. Redistribution of the plasma density by the propagating pulse leads to

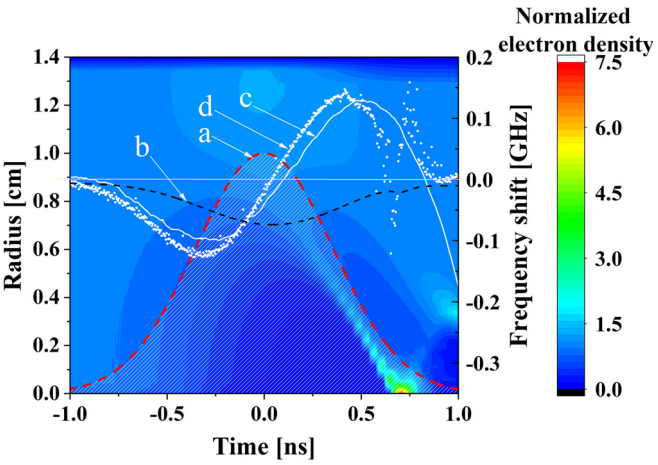

FIG. 7. Electron density perturbation and frequencies associated with the wake. (a) The envelope of the pulse power; (b) the eigen-frequency shift, $\Delta\omega_0$, calculated using Eq. (6); (c) the local frequency shift $\Delta\omega$ of the pulse, calculated using Eq. (6); and (d) the local frequency shift $\Delta\omega$ calculated by wavelet analysis of the pulse's electric field component at a distance of 20 cm from the waveguide's input, using the LSP simulation results for an initial plasma density of 3×10^{10} cm^{-3}.

the variation of this eigen-frequency in time and along the axial coordinate, z, so that $\omega_0 = \omega_0(t, z)$.

Variation of the frequency of the electromagnetic wave propagating through the medium whose local dispersion characteristics are defined by Eq. (1) with the time-dependent parameter $\omega_0(t, z)$, is described by the following equation[15]

$$\frac{\partial\omega^2}{\partial t} + v_g\frac{\partial\omega^2}{\partial z} = \frac{\partial\omega_0^2}{\partial t}, \tag{2}$$

where v_g is the wave's group velocity. Equation (2) is valid when the characteristic temporal and spatial scales of the medium variation are large compared to the wave's period and wavelength, respectively.

Perturbation of the electron density n_e by the electromagnetic pulse propagates as a wake wave together with the pulse, i.e., with the group velocity v_g

$$n_e(t, z; r) = n_e\left(\frac{t}{v_g} - z; r\right). \tag{3}$$

This means that $\omega_0(t, z) = \omega_0\left(t/v_g - z\right)$ is constant along the characteristic of Eq. (2). Thus, Eq. (2) can be written in the form

$$\frac{d\omega^2(t)}{dt} = \left.\frac{\partial\omega_0^2}{\partial t}\right|_{t_0}. \tag{4}$$

Here, $\omega(t)$ is the local frequency of the pulse segment, which is injected into the system through the cross section $z = 0$ at the time t_0. Equation (4) means that the frequency shift, $\Delta\omega^2 = \omega^2(t) - \omega^2(t_0)$ grows linearly with the distance traveled by the pulse along the waveguide.

The change in the eigen-frequency of a cavity due to a perturbation of the material (plasma) characteristics within the cavity is described by the following expression (see, e.g., Ref. 26):

$$\frac{\omega_0 - \omega_{00}}{\omega_0} \cong -\frac{\int dV\left(\Delta\varepsilon|E_0^2| + \Delta\mu|H_0^2|\right)}{\int dV\left(\varepsilon|E_0^2| + \mu|H_0^2|\right)}, \tag{5}$$

where $\Delta\varepsilon$ and $\Delta\mu$ are the perturbations of the permittivity ε and the permeability μ, respectively. Here, it is assumed that the eigen-frequency ω_{00} and the electric and magnetic fields $\vec{E}_0$ and $\vec{H}_0$ of the eigen-mode of the unperturbed cavity are known and that these perturbations are very small.

For the case being considered, $\mu = 1$ and $\varepsilon = 1 - 4\pi e^2 n_e(r)/m\omega^2$, so that

$$\frac{\Delta\omega_0}{\omega_0} \cong \frac{\omega_{p0}^2}{\omega_0^2} \frac{\int rdr\left[1 - \frac{n_e(r)}{n_0}\right]E_0^2(r)}{\int rdr\left[\left(1 - \frac{\omega_{p0}^2}{\omega_0^2}\right)E_0^2(r) + H_0^2(r)\right]}. \tag{6}$$

The electron density evolution during the HPM pulse propagation was calculated using the 1D model of Ref. 7 and the frequency shift was calculated using Eqs. (4) and (6). Because the 1D model does not take into account the pulse frequency variations, 3D LSP simulations were used to verify this model. The results of this comparison are shown in Fig. 7. It should be pointed out that the frequency's temporal variation, presented here, is similar to that obtained in Ref. 21, in spite of the difference in the geometry of the problems considered. One can see that the wake excitation leads to a local frequency shift of the pulse, that is, the frequency of the leading part of the pulse is down-shifted, while its rear part is up-shifted. Consequently, the group velocity of the leading part is smaller than the group velocity of the rear part. This results in a decrease in the pulse's natural spread or can even lead to pulse compression. As an example, the pulse envelope's evolution while propagating in a vacuum and in a plasma filled waveguide are compared in Fig. 8(a).

Thus, the experimentally observed pulse compression, can be explained by the wave frequency's self-modulation caused by the wake excitation in the plasma. The compression degree depends on the parameters of the system such as the pulse power, plasma density, length of the plasma-filled part of the waveguide, etc. For example, in the experiment, the downstream half of the flashboard plasma sources was turned off so that the plasma filled only the upstream half of the waveguide. The experimental results in Fig. 8(b) demonstrate that pulse compression and increase in the power in ~1.5 are enhanced compared with full-length plasma filling where the increase in power due to the pulse compression was ≤1.2 (see Fig. 6). The dependence of the wake excited HPM pulse compression on various parameters will be studied in detail in future research.

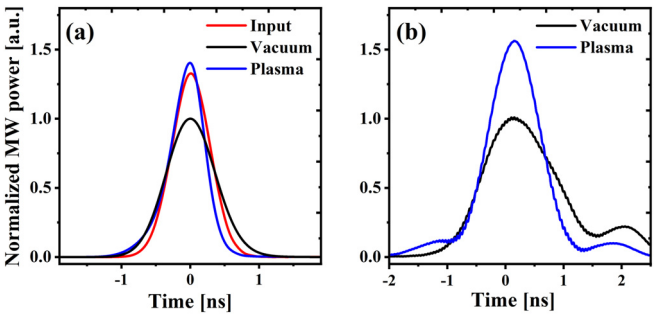

FIG. 8. (a) LSP pulse envelope at the waveguide input (red) ($z = 0$) and calculated at a distance of 60 cm in a 3×10^{10} cm^{-3} density plasma (blue) and in a vacuum (black); (b) experimentally observed pulse envelopes measured by coupler #2 for the vacuum (red) and when the plasma (10^{11} cm^{-3}) fills only the upstream half of the waveguide (black). All values are related to the normalized maximum of the power signal measured at the exit in the vacuum.

B. Fast electron flux through the waveguide's side boundary

The HPM pulse ejects part of the plasma electrons through the waveguide wall, which is semi-transparent for electrons and opaque for the microwave field. These free-propagating electrons can be registered near the chamber wall as described in Sec. III. Using the 1D model, the energy of all electrons in the waveguide cross section and electrons penetrating through the waveguide boundary as a function of time is plotted in Fig. 9. The electron energy distribution pattern lags slightly behind the HPM power profile and fluctuates with the HPM frequency with increasingly high energies. The high energy electrons reaching ~50 keV oscillate within the interior of the waveguide cross section and do not reach the waveguide boundary. There are two groups of electrons which leave the waveguide through its boundary. The *first* group appears as the HPM pulse rises and can reach ~5 keV. These are electrons which have reached sufficient energy in the outward direction before they are attracted back toward the center where a net positive ion charge is building up. The *second* group of electrons appears at the tail of the HPM pulse and reaches higher energies of ~15 keV. During the propagation of the HPM pulse, the ponderomotive forces push electrons out toward the waveguide wall leaving a positively charged interior region. As these electrons slow down and concentrate near the wall, as the HPM pulse nears its tail, these electrons are re-attracted by the positive ion space charge and focus near the axis. This focusing toward the axis is accompanied by electron density fluctuations accompanied by electric fields which enhance near the axis. During this non-stationary electron focusing phase, some electrons can reach energies high enough to overcome the attracting ion space charge potential barrier and eject toward the waveguide boundary.

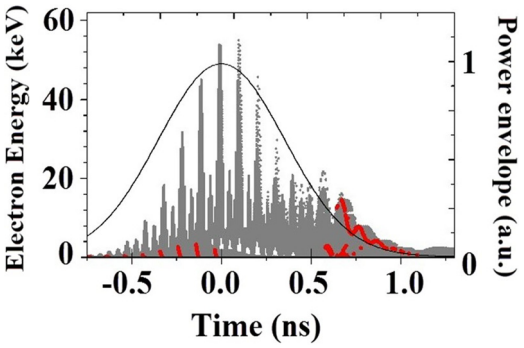

FIG. 9. Energies of all electrons in the waveguide cross section vs time calculated by the 1D model (gray), electrons that penetrate through the waveguide boundary (red), and the envelope of the pulse power (black curve) for a plasma density of 5×10^{10} cm^{-3}. Time is measured relative to the maximum of the power.

The results of the 1D model in Fig. 9 reproduce the experimentally measured induced light signal observed by the side fiber in Fig. 4 at the tail of the HPM pulse confirming the scenario described. Using various thickness Al foils to cover the fiber opening prevents the measurement of the first group electrons.

In Fig. 10, the results of 3D LSP calculations for a $3 \times 10^{10}\,\mathrm{cm}^{-3}$ density plasma filled 1.4 cm radius waveguide are presented. In Fig. 10(a), one can see a snapshot at $t = 2.4$ ns of the plasma density modulation seen in the $[x, z]$ plane of the 3D volume, caused by a 0.5 GW, HPM pulse whose time envelope is Gaussian with 0.6 ns (FWHM). (Note that in contrast to the 1D model (Fig. 9), in the PIC calculations $t = 0$ corresponds to the HPM pulse's injection time at $z = 0$). In Fig. 10, the HPM pulse's maximum is at $z = 15$ cm. As the HPM pulse propagates along the waveguide, plasma electrons are forced toward the waveguide walls leaving a net positively charged island in the central region [Fig. 10(a)]. Electrons concentrate near the walls reaching a density more than twice the initial uniform density, n_e^0. In the wake at the pulse's tail, electrons concentrate to densities up to five times n_e^0. This plasma density modulation is similar to that observed in the laser-plasma produced wake (Ref. 4). Figure 10(b) depicts the energies of the plasma electrons along the axial coordinate z. Energies can reach values up to ~35 keV at $z \sim 15$ cm at the maximum of the power of the HPM pulse. In Fig. 10(c), one can see that from the electrons in the region [14 cm $\leq z \leq$ 16 cm, black dots in Fig. 10(c)], that is, near the peak of the HPM's power, electrons which reach the waveguide walls ($r \geq 1.4$ cm) are of relatively low energy ($\leq$3 keV). Electrons collected from the tail region of the pulse [2.5 cm $\leq z <$ 14 cm, red dots in Fig. 10(c)] reach the walls with energies up to ~10 keV. These results agree with the results of the 1D model calculations (see Fig. 9).

The electrons observed in the experiment by the side viewing fibers can reach energies of ~25 keV, higher than those predicted by the 1D model [Fig. 9 and the PIC simulation results in Fig. 10(c)]. The experimental waveguide contains a low pressure neutral gas which was not accounted for so far. In Fig. 10(d), we present the same results as in Fig. 10(c), but in the LSP simulations a $5 \times 10^{14}\,\mathrm{cm}^{-3}$ density background carbon atom gas is introduced so that electron-neutral collisions and impact ionization are included. The amount of ionization is very small but the presence of collisions changes the electron energy distribution. Electrons of energy up to ~45 keV are collected on the walls and electrons within the waveguide can reach energies up to ~100 keV. One should note that these calculations are for solid wall waveguides and not the partially transparent waveguide used in the experiment.

In conclusion, the 1D model and the 3D PIC simulations allow us to connect the observation of high-energy electrons by the side viewing fibers to the dynamics of the wake formation by the HPM pulse traversing the plasma filled waveguide.

C. Wake-assisted additional ionization

Wake excitation is accompanied by either partial or even complete ejection of electrons onto the waveguide wall. As the HPM pulse

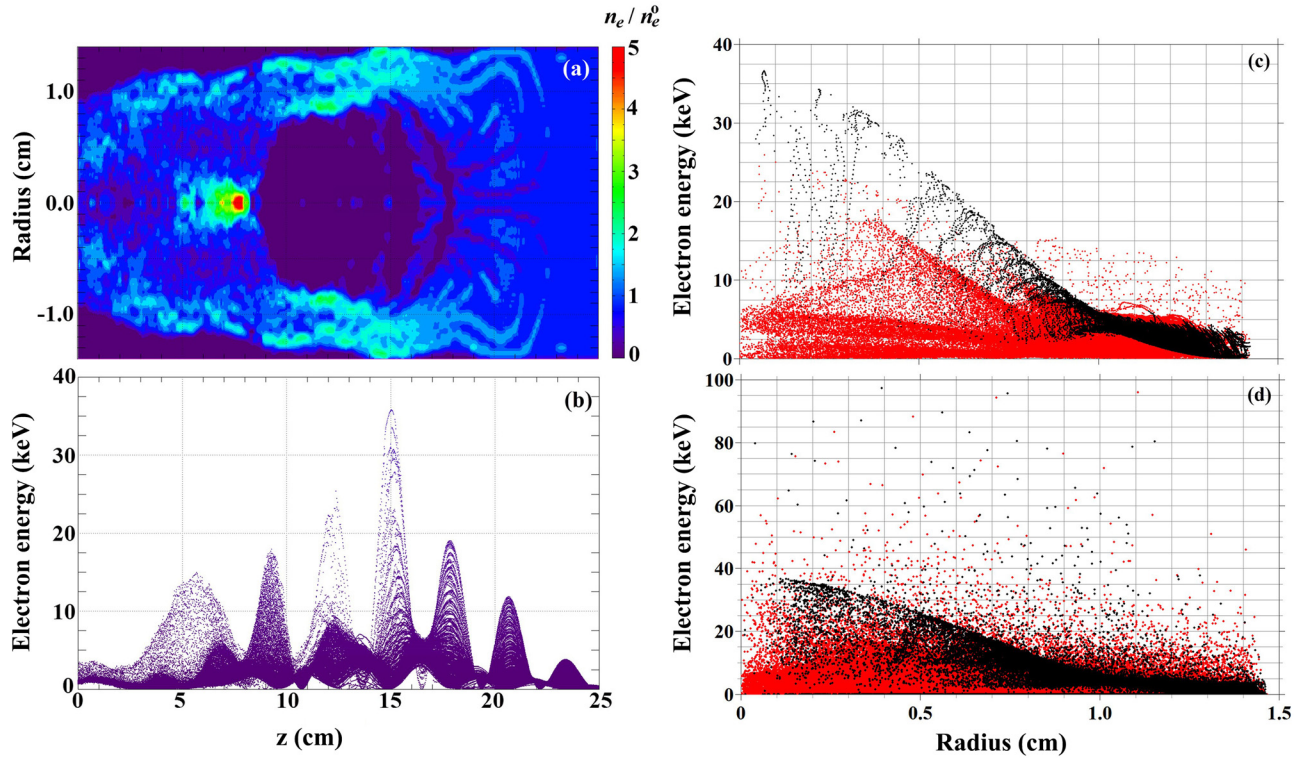

FIG. 10. LSP calculations in the Cartesian 3D space: (a) Relative electron density contours in the $[x, z]$ plane at $t = 2.4$ ns. (b) Energies of all electrons vs z at $t = 2.4$ ns. (c) Energies vs their radial position r of all electrons seen in (b) in the region 14 cm $\leq z \leq$ 16 cm (black dots) and 2.5 cm $\leq z \leq$ 14 cm (red dots). (d) Same as (c) but with collisions and ionizations included.

propagates, some of the non-compensated charge of background ions remains in the waveguide. Electrons, which remain in the waveguide, are trapped and oscillate in the potential well of this non-compensated charge. Eventually, this potential well disappears due to ion motion toward the waveguide wall (if the wall is opaque) or electrons penetrating from the exterior plasma (if the wall is semi-transparent as is the case in the experiment). Both these processes are slow and the space charge neutralization process continues long after the HPM pulse has passed through the waveguide.

The depth of the potential well, $\Delta\varphi$, (and, consequently, the possible energy of the oscillating electrons) depends on the density of the uncompensated positive ion charge, which for the experimental conditions ($R = 1.4$ cm, $n_i = ne = n0 = 3 \times 10^{10}$ cm^{-3}) can reach 26 kV, considering complete of electrons ejection from the waveguide. For incomplete ejection, the oscillating energy of the remaining electrons in the potential, is sufficient to impact ionize neutrals present in the plasma. However, this additional ionization does not change the value of uncompensated charge. Therefore, all initial and newly created electrons remain trapped in the well and spend their energy on excitation/ionization producing collisions. Thus, the HPM pulse leaves behind it a plasma density and light intensity which increases over a certain period of time followed by relaxation. The characteristic time of this light's temporal evolution can be several orders of magnitude longer than the HPM pulse duration.

Let us estimate a final value and temporal growth rate of the plasma density, using the simple model described above. Assuming that electrons and ions are homogeneously distributed over the waveguide cross section, one can calculate the waveguide's wall potential relative to the axis as

$$\Delta\varphi = \pi e R^2 (n_i - n_e), \tag{7}$$

where n_i and n_e are the ion and electron densities, respectively. One can estimate the kinetic energy of an electron oscillating in the potential well to be $w \sim e\Delta\varphi = \pi e^2 R^2 (n_i - n_e)$. Any electron can ionize $N \approx w/\varepsilon_i$ neutrals (atoms or molecules) whose ionization energy is ε_i. Thus, the density of the plasma formed by additional ionization can be estimated as $n_p \sim \left[\pi e^2 R^2 (n_i - n_e) n_e\right]/\varepsilon_i$. This density reaches its maximum at $n_e = n_i/2$

$$\max\{n_p\} \approx \frac{\pi e^2 R^2 n_i^2}{4\varepsilon_i}. \tag{8}$$

For the experimental conditions mentioned above, one obtains max $\{n_p\} \sim 10^3 n_i$. Considering that the estimate of Eq. (8) is very rough, it can be still confidently stated that the wake phenomenon can lead to the formation of a plasma exceeding considerably the initial density. Note that the final plasma density can be so large only when the HPM pulse power is large enough to eject half of the initial plasma electrons from the waveguide.

The above estimate is based on the assumption that all electrons have the same maximum allowable energy $w \sim e\Delta\varphi$ which overestimates the possible increase in the plasma density. For a more precise evaluation, it is necessary to know the energy distribution of the electrons $n_e(w)$, oscillating in the potential well.

Any ionization event is accompanied by the disappearance of a primary electron from its initial energy interval $[w, w + dw]$ and the appearance of two electrons of lower energies w_1 and w_2, where $w_1 + w_2 = w - \varepsilon_i$. For simplicity, it is assumed below that $w_1 = w_2$, so that both secondary electrons have the same energy. Thus, variation of the electron density $n_e(w)$ in a given energy interval is described as follows:

$$\frac{dn_e(w)}{dt} = -n_0 n_e(w) I(w) + 2n_0 n_e(2w + \varepsilon_i) I(2w + \varepsilon_i), \tag{9}$$

where n_0 is the density of the neutral gas, $I(w) = \sigma_i[w_k(t)]\left|v(t)\right|$ is the ionization rate with $\sigma_i[w_k(t)]$ being the ionization cross section and the electron velocity $|v| = \sqrt{2w/m}$. Equation (9) should be supplemented by the initial energy distribution of electrons $n_e^{(0)}(w)$. The energy distribution of the electrons after the HPM pulse propagation was calculated for different plasma densities using the 1D model and for a plasma density of $n_0 = 3 \times 10^{10}$ cm^{-3} using the PIC simulation results. It was found that the energy distribution is practically independent of plasma density and both the 1D model and 3D PIC simulation demonstrate very similar dependencies on energy above the ionization threshold, as it is shown in Fig. 11. It should be noted here that in the 1D model, the distribution function was calculated ~10 ns or later after the pulse has left, when oscillating electrons are sufficiently mixed, while the total duration of the 3D PIC simulation did not exceed 5–6 ns, so that the electrons' ensemble did not reach the steady-state. This can be the reason for the difference between the results of 1D and 3D PIC models.

Since the energy distribution is independent of the initial plasma density n_0, the normalized density $\eta = n(t)/n_0$ of the newly created plasma is also independent of n_0. Moreover, the intensity of light emission, registered by a side fiber, as it follows from this model, should be proportional to n_0. The numerical solution of Eq. (9) for the energy distributions shown in Fig. 11, and the calculated normalized light intensities, are presented in Fig. 12 and confirm this statement. The time dependence of the calculated light emission is similar to that seen in the experiment (Fig. 5).

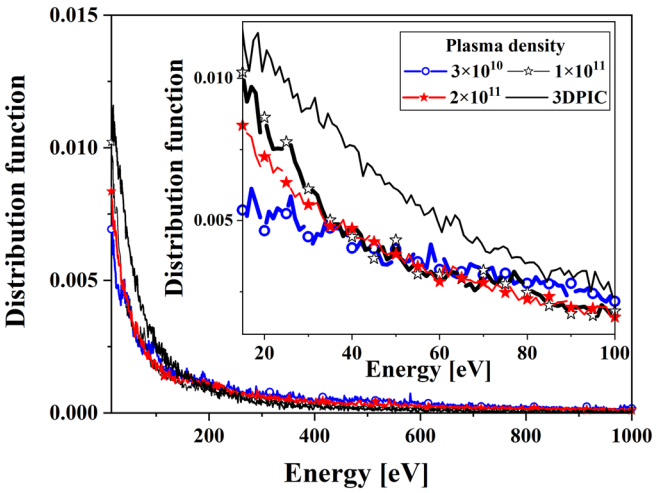

FIG. 11. Distribution functions $n_e^{(0)}(w)$ as functions of electron energy. The lines with symbols are obtained using the 1D model and the solid line is the result of the 3D PIC simulation.

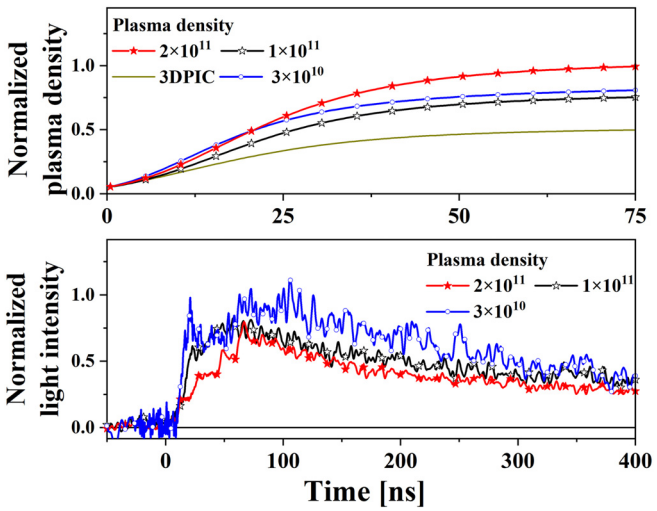

FIG. 12. (a) Calculated normalized plasma density $\eta = n(t)/n_0$ for different initial densities $n(0)$. Neutral gas (Carbon) density $n_C = 2 \times 10^{15}$ cm^{-3}. (b) Intensity of light registered by the side fiber and normalized by the initial plasma density n_0 (in arbitrary units).

3D PIC and 1D simulations show that for the experimental conditions considered, the HPM pulse ejects approximately 30%–40% of the electrons through the waveguide boundary. The remaining electrons oscillate near their equilibrium positions and to a large extent compensate the ion space charge in the waveguide interior region, so that the electric field is concentrated mainly between the waveguide boundary and the almost quasi-neutral "plasma core." This is demonstrated in Fig. 13, where a normalized distribution of the electron density across the waveguide, obtained in the 3D PIC simulation, is depicted. The electron density is almost homogeneous up to ∼9 mm and drops sharply near the waveguide wall, so that non-compensated ions form a few millimeters thick "cladding," where the electric field is concentrated.

The relative density of the ionization events is also shown in Fig. 13. The density of ionization events is the maximum on the axis and decreases gradually toward the waveguide wall. This can explain the radial profile of the light intensity, presented in Fig. 2, assuming that ionization and light emission occur in the same plasma region.

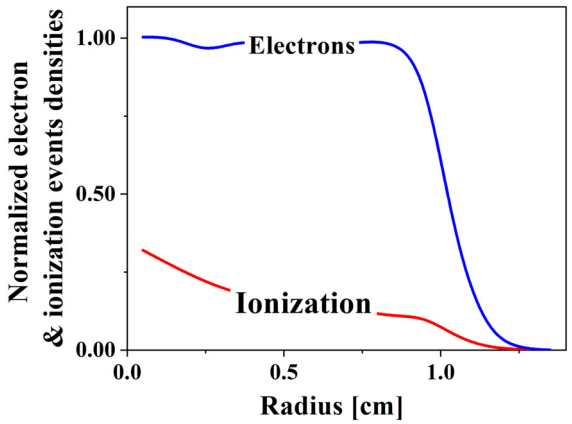

FIG. 13. Radial distributions of electrons and ionization events.

It should be noted that the electric field of the non-compensated space charge which confines the electrons, forces ions out toward the waveguide boundary which destroys the potential well for electrons and terminates ionization faster than that estimated above.

D. Electrons ejected at the downstream waveguide exit

As mentioned in Sec. IV A, the non-compensated space-charge formation in the radial direction is over a dimension much smaller than the longitudinal dimension. Consequently, the longitudinal Coulomb electric field is much smaller than the radial fields over the entire transversal cross section, apart from the region near the waveguide axis, where the radial field vanishes. Thus, to explain the electrons with energies of several tens keV up to ∼100 keV (see Fig. 3), registered in the experiment by the Faraday cup or fiber placed 5–10 cm from the waveguide exit, requires additional consideration.

We considered two possible mechanisms: (i) collisions, which allow electrons to acquire a large longitudinal velocity in the oscillating field of the HPM pulse and (ii) acceleration of electrons at the sharp output edge of the waveguide. The electromagnetic field structure and value can be very different on each side of the waveguide's radius discontinuity resulting in a net electron energy gain even in the presence of the very short oscillating electric field pulse.

The role of these two mechanisms was studied by 3D LSP simulations in waveguides of two different geometries. First, we consider a uniform (U) transition (in radius) between the waveguide's plasma filled region and the vacuum which extends to the Faraday cup or fiber. Second, we model the existing non-uniform (NU) sudden radius increase from 1.4 cm to 6.5 cm beyond the plasma edge. For both geometries, collisions and ionizations were either included (I) or not included (NI) in the simulations. We assume that the background neutral gas is mainly carbon atoms of 5×10^{14} cm^{-3} density. The results of these simulations are shown in Fig. 14, where tracks of electrons ejected downstream from the plasma-filled region toward the Faraday cup are depicted.

In Fig. 14, the particle tracks are recorded over a 10 cm long vacuum section following the plasma filled waveguide from the time the HPM pulse reaches the edge of the plasma up to the time the pulse has left the edge of the interval considered. The effect of both mechanisms (NU and I) considered is clearly seen in Fig. 14. Both cause electrons to be ejected to longer distances. In Fig. 14, because of overlapping trajectories, it is difficult to discern the particle energies but the highest energies particles can achieve (>100 keV) are for the case where both mechanisms are present in the simulation. These results confirm that the sudden radial transition in the tube connected at the end of the plasma filled waveguide and collisions is responsible for the high energy electrons observed in the experiment.

V. SUMMARY

Some peculiar features of the wake excited by a powerful short microwave pulse in a plasma-filled waveguide, have been studied experimentally, theoretically, and numerically. Such features are weak or even absent in transversally-unbound plasma. The use of various experimental diagnostics, theoretical modeling, and numerical

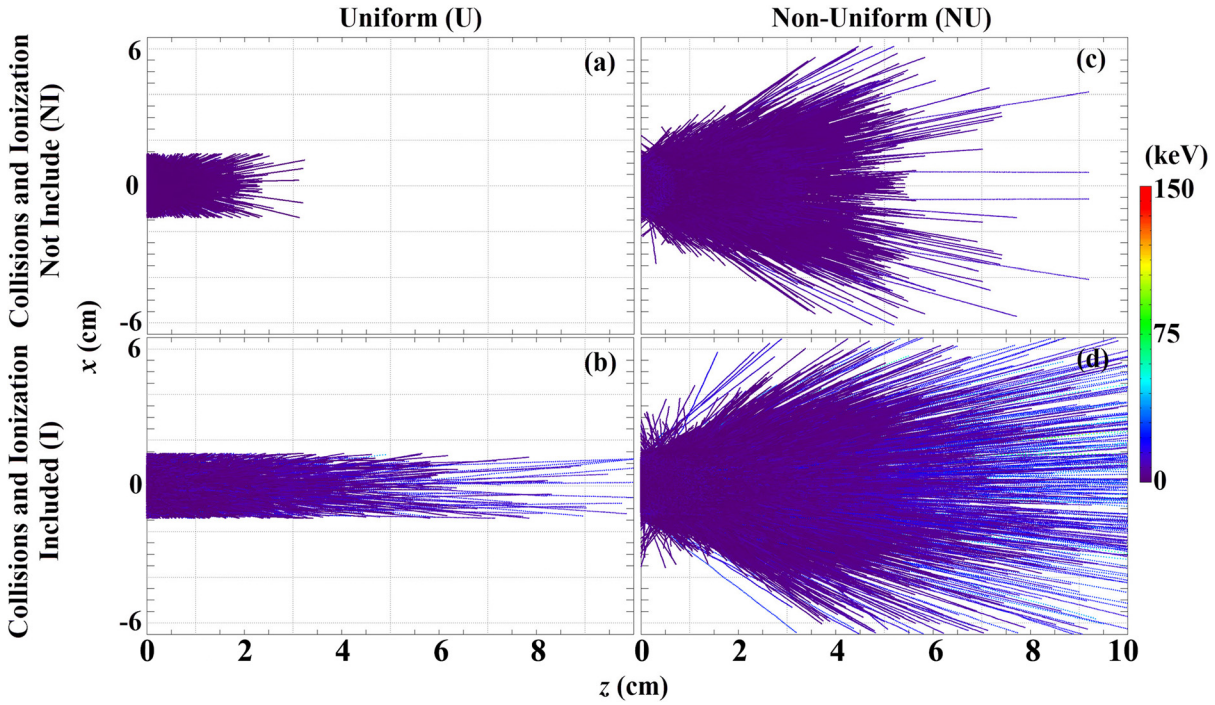

FIG. 14. Trajectories of electrons ejected from the plasma edge ($z = 0$ cm) into space toward the FC. In (a) and (c), collisions and ionizations are not included (NI), whereas and in (b) and (d), they are included (I). In (a) and (b), there is no radial transition between the plasma filled waveguide and the exit tube. In (c) and (d), the waveguide radius increases sharply from 1.4 cm to 6.5 cm at $z = 0$ cm.

simulations allows us to associate the experimental data with physical phenomena related to the wake formation in plasma during the pulse propagation and long time after its passage. Transversal redistribution of the plasma density, caused by the ponderomotive force, modifies the local frequency of the pulse in such a way that the group velocity of the pulse's rear becomes larger than the group velocity at its front, leading to pulse compression. This theoretical result is confirmed experimentally. Note that in a transversally-unbound plasma, this effect is much smaller because the dependence of the group velocity on plasma density in a waveguide is much stronger, especially close to the cut-off frequency.

The ponderomotive force of the pulse ejects part of the plasma electrons to the waveguide boundary, whereas plasma ions remain practically immobile, forming a Coulomb potential well for the remaining electrons. The formation of a positively-charged plasma behind the electromagnetic pulse is impossible in a transversally-unbound plasma. Electrons trapped in the well possess quite a large energy, several kilo electron volts and more, and ionize the neutral background gas present in the waveguide. Ionization continues during several tens of nanoseconds and increases the plasma density many times. This scenario is responsible for a long time, up to hundreds of nanoseconds, plasma light emission.

The observed HPM pulse compression and the detection of fast electrons penetrating the wire boundary of the waveguide and at the waveguide output indicate unambiguously that a wake is indeed effectively excited by the HPM pulse propagating in the plasma-filled waveguide. The observed short- and long- time observations confirm the suggested theoretical models and the results of the numerical simulations.

ACKNOWLEDGMENTS

The authors are grateful to S. Gleizer and E. Flyat for their technical help without which this research could not have been performed. This study was supported by the Pazy foundation Grant No. 2025988.

DATA AVAILABILITY

The data that support the findings of this study is available from the corresponding author upon reasonable request.

REFERENCES

[1]A. A. Eltchaninov, S. D. Korovin, G. A. Mesyats, I. V. Pegel, V. V. Rostov, V. G. Shpak, and M. I. Yalandin, IEEE Trans. Plasma Sci. **32**, 1093 (2004).
[2]G. Shafir, Y. E. Krasik, Y. P. Bliokh, D. Levko, Y. Cao, J. G. Leopold, R. Gad, V. Bernshtam, and A. Fisher, Phys. Rev. Lett. **120**, 135003 (2018).
[3]T. Tajima and J. M. Dawson, Phys. Rev. Lett. **43**, 267 (1979).
[4]E. Esarey, C. B. Schroeder, and W. P. Leemans, Rev. Mod. Phys. **81**, 1229 (2009).
[5]Y. Cao, J. G. Leopold, Y. P. Bliokh, A. Li, G. Shafir, A. Fisher, G. Leibovitch, V. V. Rostov, and Y. E. Krasik, IEEE Trans. Plasma Sci. **48**, 792 (2020).
[6]H. K. Malik, S. Kumar, and K. P. Singh, Laser Part. Beams **26**, 197 (2008).
[7]Y. P. Bliokh, J. G. Leopold, G. Shafir, A. Shlapakovski, and Y. E. Krasik, Phys. Plasmas **24**, 063112 (2017).
[8]Y. Cao, Y. Bliokh, J. G. Leopold, V. Rostov, Y. Slutsker, and Y. E. Krasik, Phys. Plasmas **26**, 023102 (2019).

[9]G. Shafir, A. Shlapakovski, M. Siman-Tov, Y. Bliokh, J. G. Leopold, S. Gleizer, R. Gad, V. V. Rostov, and Y. E. Krasik, J. Appl. Phys. **121**, 033301 (2017).
[10]L. M. Earley, W. P. Ballard, and C. B. Wharton, IEEE Trans. Nucl. Sci. **32**, 2921 (1985).
[11]M. J. Berger, J. S. Coursey, M. A. Zucker, and J. Chang, "Stopping-power and range tables for electrons, protons, and helium ions," NIST Standard Reference Database 124 (Physical Measurement Laboratory, 2017).
[12]D. R. Welch, D. V. Rose, B. V. Oliver, and R. E. Clark, Nucl. Instrum. Methods Phys. Res., Sect. A **464**, 134 (2001).
[13]D. R. Welch, D. V. Rose, M. E. Cuneo, R. B. Campbell, and T. A. Mehlhorn, Phys. Plasmas **13**, 063105 (2006).
[14]E. Yablonovitch, Phys. Rev. A **10**, 1888 (1974).
[15]V. B. Gildenburg, V. A. Krupnov, and V. E. Semonov, Sov. Tech. Phys. Lett. **14**, 738 (1988).
[16]S. P. Kuo, Phys. Rev. Lett. **65**, 1000 (1990).
[17]E. Esarey, G. Joyce, and P. Sprangle, Phys. Rev. A **44**, 3908 (1991).
[18]A. Giulietti, A. André, S. Dobosz Dufrénoy, D. Giulietti, T. Hosokai, P. Koester, H. Kotaki, L. Labate, T. Levato, R. Nuter, N. C. Pathak, P. Monot, and L. A. Gizzi, Phys. Plasmas **20**, 082307 (2013).
[19]J. K. Koga, N. Naumova, M. Kando, L. N. Tsintsadze, K. Nakajima, S. V. Bulanov, H. Dewa, H. Kotaki, and T. Tajima, Phys. Plasmas **7**, 5223 (2000).
[20]M. A. Gaafar, T. Baba, M. Eich, and A. Y. Petrov, Nat. Photonics **13**, 737 (2019).
[21]J. M. Dias, L. Oliveira e Silva, and J. T. Mendonça, Phys. Rev. Spec. Top. -Accel. Beams **1**, 31301 (1998).
[22]C. D. Murphy, R. Trines, J. Vieira, A. J. W. Reitsma, R. Bingham, J. L. Collier, E. J. Divall, P. S. Foster, C. J. Hooker, A. J. Langley, P. A. Norreys, R. A. Fonseca, F. Fiuza, L. O. Silva, J. T. Mendoņa, W. B. Mori, J. G. Gallacher, R. Viskup, D. A. Jaroszynski, S. P. D. Mangles, A. G. R. Thomas, K. Krushelnick, and Z. Najmudin, Phys. Plasmas **13**, 033108 (2006).
[23]W. P. Leemans, C. W. Siders, E. Esarey, N. E. Andreev, G. Shvets, and W. B. Mori, IEEE Trans. Plasma Sci. **24**, 331 (1996).
[24]C. Ren, B. J. Duda, R. G. Hemker, W. B. Mori, T. Katsouleas, T. M. Antonsen, and P. Mora, Phys. Rev. E **63**, 026411 (2001).
[25]O. Shorokhov, A. Pukhov, and I. Kostyukov, Phys. Rev. Lett. **91**, 265002 (2003).
[26]R. F. Harrington, *Time-Harmonic Electromagnetic Fields* (John Wiley and Sons, Inc., 2001).